Environmentally-induced loss of performance in FRP strengthening systems bonded to full-scale masonry structures

This is the final peer-reviewed accepted manuscript of:

Antonio Maria D'Altri, Stefano de Miranda, *Environmentally-induced loss of performance in FRP strengthening systems bonded to full-scale masonry structures*, Construction and Building Materials, Volume 249, 2020, 118757

ISSN 0950-0618

The final published version is available online at: https://doi.org/10.1016/j.conbuildmat.2020.118757

Environmentally-induced loss of performance in FRP strengthening systems bonded to full-scale masonry structures

Antonio Maria D'Altri, Stefano de Miranda*

Department of Civil, Chemical, Environmental, and Materials Engineering (DICAM), University of Bologna, Viale del Risorgimento 2, Bologna 40136, Italy

*corresponding author: stefano.demiranda@unibo.it

GRAPHICAL ABSTRACT

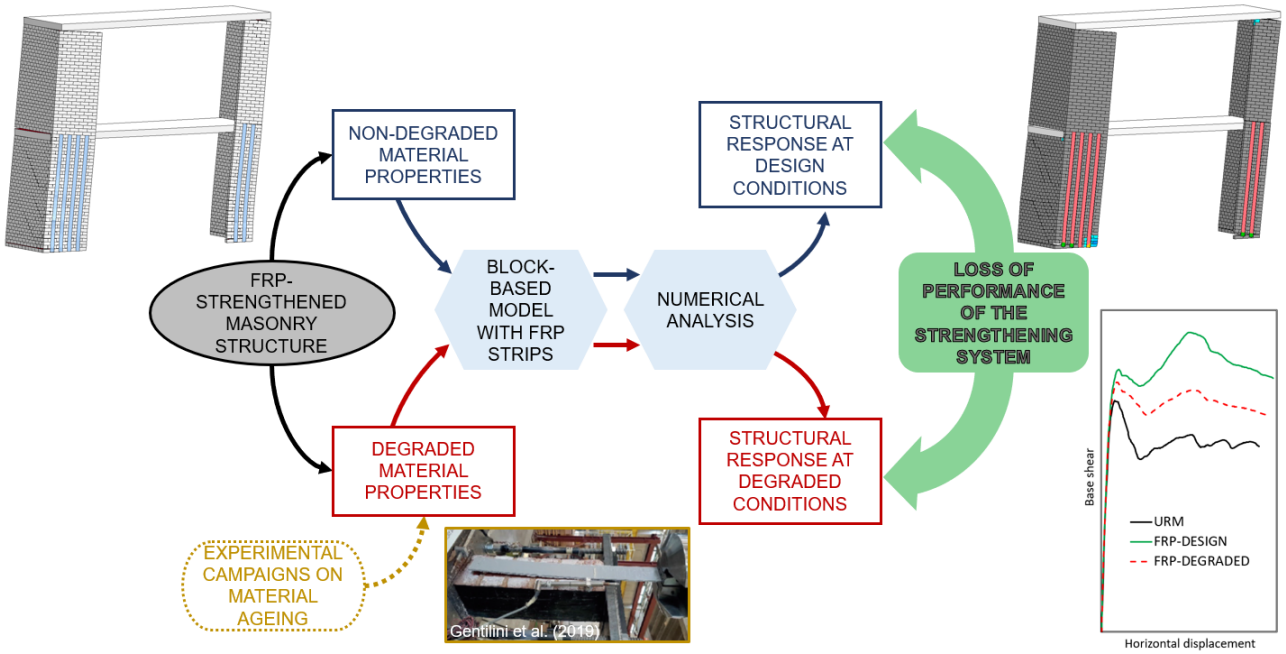

ABSTRACT

The issue of building materials deterioration due to environmental actions, which are expected to worsen in the future according to climate change predictions, is recognized as high-priority by the scientific community. However, the impact of material deterioration on the structural and seismic performances of masonry and historical structures strengthened with composites has not been investigated in detail, even though potentially significant. This paper aims to evaluate the environmentally-induced loss of performance in fiber reinforced polymer (FRP) strengthening systems bonded to masonry structures. An efficient damaging block-based modelling strategy, recently developed by the authors, is used to model masonry. FRP strips are originally introduced in the model and bonded to masonry blocks through a contact-based formulation with cohesion. This novel numerical approach is validated through FRP-strengthened masonry wall benchmarks. Numerical analyses are performed on FRP-strengthened in- and out-of-plane loaded masonry full-scale walls and houses with non-degraded material properties to predict the structural response at design conditions. Then, degraded material properties are deduced from accelerated ageing laboratory tests which investigated environmental degradation in FRP-strengthened masonry and are adopted in the same numerical analysis framework to predict the structural response at degraded conditions. Therefore, the environmentally-induced loss of performance in FRP strengthening systems bonded to masonry structures is deduced by comparing the structural response at degraded conditions with the one at design conditions.

Keywords: Masonry; Fiber reinforced polymer; Environmental ageing; Block-based model; Durability

1 Introduction

Masonry and historical structures, although typically stable under dead loads, generally show very weak performances when subjected to earthquakes. This happens mainly due to the nature of the masonry material, i.e. characterized by low tensile and shear strengths of the block-to-block bond (mortar joints), and the quasi-brittle behaviour of blocks (bricks, stones, ashlars, etc.). Various strengthening systems have been developed to overcome these weaknesses [1] and guarantee a sufficient level of safety to existing masonry buildings. Composite strengthening systems, i.e. fiber reinforced polymer (FRP), fiber reinforced cementitious matrix (FRCM), and steel reinforced grout (SRG), found an extensive application on masonry structures due to their favourable and appealing features [2].

The scientific community devoted a considerable effort to the mechanical understanding and characterization of these composite systems bonded to masonry [3]. In this context, FRP-based systems have the longest tradition, as they have been studied for more than 20 years [4, 5, 6]. Indeed, many experimental studies [7, 8, 9, 10, 11, 12, 13, 14, 15, 16] have been conducted, in addition to several analytical [17, 18, 19, 20] and numerical [21, 22, 23, 24, 25, 26, 27] solutions that have been proposed for FRP-strengthened masonry.

Although the mechanics of masonry strengthened with FRP has been copiously studied in the last two decades [28], the issue of its durability has been only more recently investigated [29], and some aspects still appear scarcely understood. Indeed, few experimental campaigns have been specifically conducted to evaluate the potential environmentally-induced degradation of FRP strengthening systems bonded to masonry. Particularly, the effects of salt decay [30, 31, 32] and thermo-hygrometric ageing [33, 34, 35, 36, 37, 38, 39] on the FRP-masonry bond have been investigated through pull-off and single-lap shear tests after accelerated laboratory conditioning of the specimens. The aspect of environmental degradation [40] becomes even more important in view of the expected future worsening of environmental actions according to climate change predictions [41, 42].

However, the impact of material deterioration on the structural and seismic performances of FRP-strengthened masonry structures has not been investigated at a full-scale level, even though potentially significant. Indeed, the only attempt in this direction has been carried out by Ghiassi et al. [43], using a simplified model for in-plane loaded 1:4-scale masonry walls.

This paper aims to evaluate the environmentally-induced loss of performance in FRP strengthening systems bonded to full-scale masonry structures.

To this purpose, firstly a new numerical strategy to model the in- and out-of-plane mechanical response of FRP-strengthened masonry is set-up. Particularly, the block-based model recently developed by the authors in [44] for unreinforced masonry is extended to the FRP-strengthened case by employing a contact-based formulation with cohesion for the bonding between masonry and FRP.

This novel numerical model to simulate FRP-strengthened masonry is validated through the comparison with experimental and other numerical outcomes available in the literature. Particularly, well-known in-plane and out-of-plane benchmarks [45, 46], which have been widely used in various scientific works to validate numerical models for FRP-strengthened masonry, are selected and used for comparisons. Accordingly, no environmentally-induced degradation is considered within this section, as the validation of the model is already an original aspect of this research.

The proposed numerical model is then used for further predictions, i.e. to evaluate the environmentally-induced loss of performance in FRP strengthening systems bonded to masonry structures. Firstly, numerical analyses are performed with non-degraded material properties to predict the structural response at design conditions. Then, degraded material properties are deduced from accelerated ageing laboratory tests which investigated environmental degradation in FRP-strengthened masonry and are adopted in the same numerical analysis framework to predict the structural response at degraded conditions. Therefore, the environmentally-induced loss of performance in FRP strengthening systems bonded to masonry structures is deduced by comparing the structural response at degraded conditions with the one at design conditions. The potential of this approach is

assessed for FRP-strengthened in- and out-of-plane loaded full-scale masonry walls and houses, where design and degraded conditions are compared for each case.

The paper is organized as follows. Section 2 reviews the state-of-the-art about experiments on environmental degradation in FRP-strengthened masonry. The proposed numerical modelling strategy for FRP-strengthened masonry is described in Section 3 and its validation in Section 4. Section 5 presents the procedure and some examples (up to a full-scale masonry terraced house) for the evaluation of environmentally-induced loss of performance in FRP strengthening systems bonded to masonry structures. Finally, Section 6 highlights the conclusions of this research work.

2 Review of experiments on environmental degradation in FRP-strengthened masonry

This section reviews the experiments on environmentally-induced degradation in FRP strengthening systems bonded to masonry. Particularly, the experimental campaigns which conceived single-lap shear tests to characterize the FRP-masonry bond have been considered herein.

In [31], Gentilini et al. presented an investigation on influence of salt attack on the stress transfer between the FRP composite and the masonry substrate. Particularly, FRP-masonry joints were subjected to salt crystallization cycles (with sodium chloride and sodium sulphate decahydrate) according to a conditioning procedure designed by the authors. After conditioning, direct shear tests were conducted on the masonry joints to investigate the interfacial bond between the substrate and the composite, showing, however, a non-significant variation in the debonding force.

In [33], Sciolti et al. analysed the influence of the ageing (immersion in water) on the FRP-masonry bond, observing a reduction of the bond strength (up to 26%) as well as a similar decrease of the maximum bond stress and a more fragile behaviour for the conditioned specimens. Successively, the effects of a thermo-hygrometric ageing on the FRP-calcareous natural stone interface behaviour was investigated by Sciolti et al. in [34]. Different failure modes were observed when passing from unconditioned to conditioned specimens. The debonding force, the maximum bond stress and the interface stiffness were affected by the treatment, manly depending on the adhesive resin deterioration.

In [37], Ghiassi et al. discussed the results of an experimental investigation on the effects of moisture on the bond behaviour in FRP-strengthened masonry. Shear bond tests showed that the ductility of the bond behaviour increased along with the conditioning, while the bond strength and stiffness were observed to decrease. Successively, in [36, 38] Ghiassi et al. discussed the results of an experimental program aimed at investigating the hygrothermal durability of bond in FRP-strengthened bricks. Accelerated ageing tests were performed on FRP-strengthened bricks, following two different hygrothermal conditioning schemes consisting of thermal cycles from (i) –10 to +50°C (90 % RH) and (ii) –10 to +30°C (90 % RH). The bond degradation was periodically investigated by visual inspection and by conventional single-lap shear bond tests. The hygrothermal exposures did not affect the mechanical properties of bricks. A progressive degradation of bond strength and fracture energy was observed in the specimens for both exposure types, although more severe in the specimens subjected to the first conditioning scheme. The failure mode changed progressively from cohesive failure in the brick to adhesive failure at the FRP-brick interface with exposure time. Additionally, an experimental investigation on the effect of long-term water immersion on the performance of GFRP-strengthened bricks was presented in [35] by Maljaee et al. The influence of mechanical surface treatment on the bond and material properties were also investigated. The single-lap shear bond tests showed a significant improvement in durability of specimens prepared with treated bricks. The failure mode of the treated specimens remained cohesive with immersion time, while the failure mode in non-treated specimens changed progressively from cohesive to adhesive failure mode.

The main outcomes of the experimental campaigns described above are summarized in Table 1, where ΔP_{MAX}^{FRP} indicates the variation of FRP-masonry debonding force due to environmental degradation, ΔG_{II}^{FRP} indicates the variation of FRP-masonry bond Mode II fracture energy, Δf_s^{FRP} indicates the variation of FRP-masonry bond strength, ΔK_{ss}^{FRP} indicates the variation of FRP-masonry bond stiffness, and ΔE^{FRP} indicates the variation of FRP Young's modulus.

Table 1. Experimental insights on FRP-strengthened masonry environmental degradation.

Reference	Conditioning	Degradation
Gentilini et al. [31]	6 cycles (96 h each) in a saline solution (20°C for 48 h) and in the oven (40°C for 48 h)	$\Delta P_{MAX}^{FRP} = -13.5\%$
Maljaee et al. [35]	Immersion in water for 12 months (20°C)	$\Delta P_{MAX}^{FRP} = -33\%$ $\Delta G_{II}^{FRP} = -49\%$ Block properties (clay brick): % variation of compressive strength $= -12\%$
Sciolti et al. [34]	32-week exposure at 40°C and 90% RH	$\Delta P_{MAX}^{FRP} = -20\%$ $\Delta f_s^{FRP} = -40\%$ $\Delta K_{ss}^{FRP} = -16\%$ Block properties (Neapolitan tuff): % variation of compressive strength $= -20\%$ % variation of flexural strength $= -70\%$
Ghiassi et al. [38] Ghiassi et al. [36]	225 cycles (6 h each) from +10 to +50°C and 90% RH	$\Delta E^{FRP} = -27\%$ $\Delta P_{MAX}^{FRP} = -45\%$ $\Delta G_{II}^{FRP} = -60\%$ No significant changes in block properties (clay brick)
Ghiassi et al. [37]	Immersion in deionized water for 24 weeks (23°C)	$\Delta E^{FRP} = -38\%$ $\Delta P_{MAX}^{FRP} = -35\%$ $\Delta K_{ss}^{FRP} = -80\%$ $\Delta G_{II}^{FRP} = -40\%$ Block properties (handmade clay brick): % variation of compressive strength $= -25\%$
Sciolti et al. [33]	Immersion in deionized water for 25 weeks (23°C)	$\Delta P_{MAX}^{FRP} - 26\%$ $\Delta f_s^{FRP} - 26\%$ % variation of block properties (Lecce stone) $= -50\%$ (compressive strength, flexural strength, and elastic modulus)

3 Numerical modelling strategy

In this section, the modelling strategy developed for the block-based analysis of FRP-strengthened masonry is described. Particularly, the block-based modelling strategy recently developed by the authors in [44], where the blocks are conceived through solid damaging FEs, is used to model masonry. Additionally, FRP strips are originally introduced in the model and bonded to masonry blocks through a contact-based formulation with cohesion.

The numerical modelling strategy developed herein for the mechanical analysis of FRP-strengthened masonry structures is sketched in Fig. 1. The damaging block-based approach proposed by the authors in [44] is utilized to model masonry, whereas linear elastic membranes, interacting with masonry blocks through a contact formulation with cohesion, are used to model FRP strips bonded to masonry (Fig. 1).

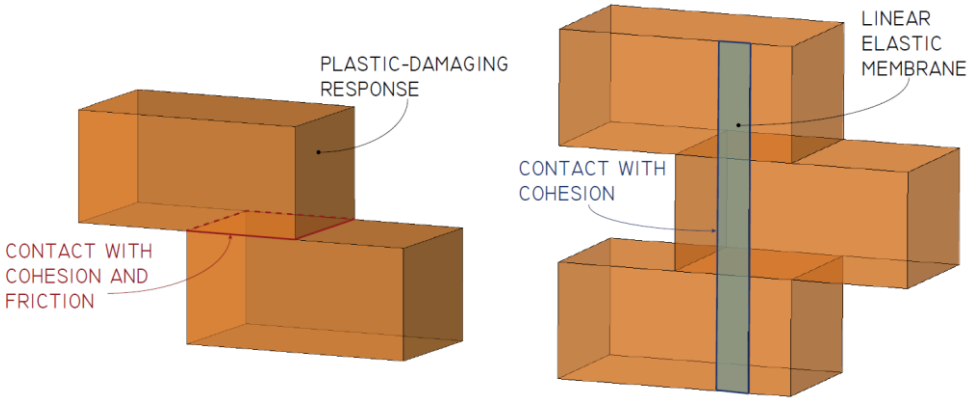

Fig. 1 – Block-based numerical modelling strategy for FRP-strengthened masonry structures.

3.1 Block-based modelling of masonry

A compatible FE mesh is adopted within the masonry block. The isotropic continuum plastic-damage constitutive model originally developed in [47] is herein utilized for the blocks. This model considers a yielding function with two hardening variables and two independent damage variables for tensile ($0 \leq d_t < 1$) and compressive ($0 \leq d_c < 1$) damage, leading to the following stress-strain uniaxial relations in tension σ_t and compression σ_c:

$$\sigma_t = (1 - d_t)E^B\left(\varepsilon_t - \varepsilon_t^p\right), \qquad \sigma_c = (1 - d_c)E^B\left(\varepsilon_c - \varepsilon_c^p\right), \tag{1}$$

where E^B is the undamaged Young's modulus of the block, ε_t and ε_c are the tensile and compressive uniaxial strains, and ε_t^p and ε_c^p are the tensile and compressive uniaxial plastic strains. The model is conceived in the framework of nonassociated plasticity [47]. Thus, the plastic potential is governed by the dilatancy angle ψ, typically assumed equal to 10° for quasi-brittle materials such as brick and stone blocks, as well as by a smoothing parameter ϵ usually assumed equal to 0.1 [48]. Furthermore, the strength domain is defined by the ratio f_{b0}/f_{c0} between the initial biaxial f_{b0} and uniaxial f_{c0} compressive strengths, usually adopted equal to 1.16 [48], and by the shape parameter ρ, typically assumed equal to 2/3 [47]. The parameters characterizing the blocks plastic-damaging behaviour are collected in Table 2, and are integrated with the tensile and compressive uniaxial strengths (f_t^B and f_c^B) and fracture energies (G_t^B and G_c^B). Linear softening is considered in both tensile and compressive behaviours.

Table 2. General parameters for the plastic damaging behaviour.

ϵ	ψ	f_{b0}/f_{c0}	ρ
0.1	10°	1.16	2/3

The interaction between blocks is idealized through a contact formulation with cohesion and friction. In particular, the contact stress in compression is computed by means of a Lagrange multiplier contact approach (contact constraint). Conversely, the pre-failure tensile and shear stresses are computed as follows:

$$\sigma = \begin{cases} K_{nn}u, & \text{with } \sigma \geq 0 \\ \text{contact constraint}, & \text{with } \sigma < 0 \end{cases}, \qquad \tau = K_{ss}\delta \tag{2}$$

where σ is the contact normal stress (positive in tension), τ is the contact shear stress, u is the normal displacement between blocks, δ is the tangential slip between blocks, K_{nn} is the cohesive stiffness in normal direction and K_{ss} is the cohesive stiffness in shear.

Failure in the contact response occurs when the contact stresses at a contact point intersects a Mohr-Coulomb failure surface with tension cut-off. This criterion, implemented in Abaqus [49] through an automatic user-defined subroutine, can be expressed as:

$$\max\left\{\frac{\langle\sigma\rangle}{f_t}, \frac{|\tau|}{f_s(\sigma)}\right\} = 1, \tag{3}$$

where $\langle x\rangle = (|x| + x)/2$ means that a purely compressive stress state does not induce contact failure, f_t is the tensile strength and f_s is the shear strength defined as:

$$f_s(\sigma) = c - \sigma\tan\phi, \tag{4}$$

where c is the cohesion and $\tan\phi$ is the initial friction of the shear response.

The maximum normal and shear stress in a contact point are described by the relationships:

$$\sigma = \begin{cases} (1-D)f_t, & \text{with } u < u_k \\ 0, & \text{with } u \geq u_k \end{cases}, \qquad \tau = \begin{cases} (1-D)f_s(\sigma) + D\mu\langle-\sigma\rangle, & \text{with } \delta < \delta_k \\ \mu\langle-\sigma\rangle, & \text{with } \delta \geq \delta_k \end{cases} \tag{5}$$

where the contact damage scalar variable D is defined as:

$$D = \begin{cases} 0, & \text{with } u \leq u_0 \text{ and } \delta \leq \delta_0 \\ \max\begin{cases} \dfrac{u_{MAX} - u_0}{u_k - u_0}, & \text{with } u_0 < u < u_k \\ \dfrac{\delta_{MAX} - \delta_0}{\delta_k - \delta_0}, & \text{with } \delta_0 < \delta < \delta_k \end{cases} \\ 1, & \text{with } u \geq u_k \text{ or } \delta \geq \delta_k \end{cases}, \tag{6}$$

being μ the residual friction, u_0 and δ_0 the separation and the slip at the limit of the linear elastic behaviour in tension and shear, respectively, u_{MAX} and δ_{MAX} the maximum separation and the maximum slip ever experienced by the contact point, respectively, u_k and δ_k the ultimate separation and the ultimate slip of the cohesive behaviour, respectively. The cohesive behaviour in tension and shear (Fig. 2), governed by the same

contact damage scalar variable D, is conceived herein with a linear softening, see Fig. 2, although exponential softening laws can be implemented as well, e.g. see [44].

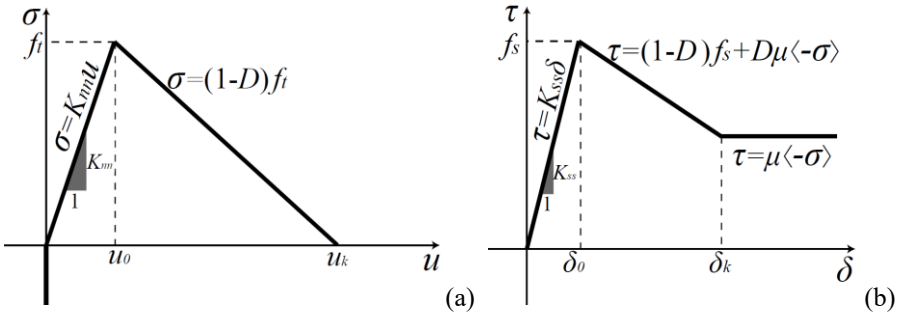

Fig. 2 – Tensile (a) and shear (b) contact behaviour between masonry blocks.

3.2 Modelling FRP reinforcement

The phenomenon of debonding between FRP and masonry substrates is complex and involves various materials (e.g. brick, mortar, primer, fibres, etc.) with different properties. This phenomenon is often characterized by the fissuring of the substrate which remains attached to the FRP strip, being the (tensile) failure in the composite uncommon, especially when the substrate is made of masonry (i.e. weak with respect to the fibres).

Therefore, here failure is supposed in the FRP-masonry bond while no failure is considered within the reinforcement. FRP strips are conceived through linear elastic membrane FEs, i.e. surface elements that transmit in-plane forces only (no moments) and have no bending stiffness, while the FRP-masonry bond is treated through a contact formulation with cohesion. Particularly, the FRP-masonry interface contact behaviour is shown in Fig. 3.

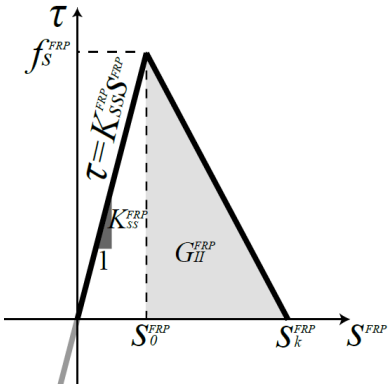

Fig. 3 – FRP-masonry interface shear contact behaviour.

The shear stress in a contact point between the FRP stirp and the masonry substrate is described by $\tau = K_{ss}^{FRP} s^{FRP}$, where K_{ss}^{FRP} is the cohesive stiffness in shear of the FRP-masonry bond, and s^{FRP} is the slip between the FRP strip and the masonry substrate, until the shear stress reaches the value f_s^{FRP}, i.e. the FRP-masonry bond strength. Then, the shear stress follows a linear softening until the ultimate slip s_k^{FRP}, governed by the Mode II fracture energy of the FRP-masonry bond G_{II}^{FRP}. The contribution of FRP strips applied on masonry substrates is typically guaranteed by the shear stress transfer between masonry and the FRP strips, thus the FRP-masonry bond is usually subjected to Mode II loads, being Mode I loads typically uncommon. Furthermore, even low in-plane compressive stresses in the FRP strips typically induce their buckling [50], due to the thinness of the strips (i.e. with no significant bending stiffness). To account for this aspect, low values of the FRP-masonry bond cohesive stiffness in normal direction are assumed (e.g. two order of

magnitude lower than the shear stiffness), and geometric nonlinearity is accounted for, so allowing the out-of-plane buckling of the strips. Finally, this modelling approach appears suitable for any kind of fibres used in the FRP, e.g. carbon fibres (CFRP) [51], glass fibres (GFRP) [52], aramid fibres (AFRP) [53] and basalt fibres (BFRP) [54].

4 Numerical model validation

The numerical model proposed in the previous section is validated through the comparison with experimental and other numerical outcomes available in the literature. Particularly, well-known in-plane and out-of-plane benchmarks [45, 46], which have been widely used in various scientific works to validate numerical models for FRP-strengthened masonry, are herein selected and used for comparisons.

4.1 Out-of-plane

The experimental tests conducted by Accardi et al. [46], also described and considered for model validation in [55, 56, 57, 58], are used herein as out-of-plane loaded masonry wall benchmark reinforced with CFRP strips (Fig. 4). Unreinforced and FRP-reinforced calcarenite ashlar masonry walls ($0.74 \times 0.21 \times 2.1$ m) are considered (Fig. 4a). The experimental tests consisted in the preliminary application of a constant 80 kN vertical force to generate vertical compression in the wall, and then in the monotonic increasing of out-of-plane horizontal displacements at the wall bottom, reproducing the conditions of a cantilever wall (i.e. fixed hinge at the top, guided support which allows only horizontal displacements at the bottom, Fig. 4b) [55]. The reinforced wall considered herein was prepared with four vertical 50 mm wide CFRP strips (0.13 mm thick) only on one side of the wall (i.e. the one subjected to vertical tensile stress). The Young's modulus of the CFRP reinforcement was 230 GPa [56]. The experimental curves obtained for the unreinforced masonry (URM) and the FRP-strengthened masonry (FRP) walls are collected in Fig. 5.

The experimental tests considered herein have been object of several numerical analyses, see for example [56, 57], were broad mechanical parameters calibration operations have been carried out to fit the experimental response. Reference to these studies have been made for the adoption of the mechanical properties. The mechanical properties used in the numerical simulations for masonry joints, blocks and FRP-masonry interfaces are collected in Table 3. Each (full) block has been discretized with 72 solid 8-node hexahedral FEs with linear shape functions. A nonlinear static analysis framework with geometric nonlinearity and imposed displacements at the wall bottom has been conceived.

Table 3. FRP-strengthened out-of-plane benchmark: mechanical parameters utilized in the numerical simulations.

Masonry joint mechanical properties (contact)		
Tensile cohesion	f_t [MPa]	0.12
Ultimate displacement of tensile cohesion	u_k [m]	$2 \cdot 10^{-4}$
Normal cohesive stiffness	K_{nn} [N/m^3]	$1 \cdot 10^{10}$
Shear cohesion	c [MPa]	0.1
Ultimate displacement of shear cohesion	δ_k [m]	$2 \cdot 10^{-4}$
Friction coefficient	$\tan \phi$ [\]	0.47
Tangential cohesive stiffness	K_{ss} [N/m^3]	$1 \cdot 10^{9}$
Masonry block mechanical properties (continuum)		
Young's modulus	E^B [MPa]	4000
Poisson's ratio	ν^B [\]	0.2
Tensile strength	f_t^B [MPa]	1.2
Fracture energy in tension	G_t^B [N/m]	$0.8 \cdot 10^{3}$
Compressive strength	f_c^B [MPa]	4
Fracture energy in compression	G_c^B [N/m]	$9 \cdot 10^{3}$
FRP-masonry interface mechanical properties (contact)		
Shear cohesion	f_s^{FRP} [MPa]	0.5
Fracture energy Mode II	G_{II}^{FRP} [N/m]	1028
Shear cohesive stiffness	K_{ss}^{FRP} [N/m^3]	$8.33 \cdot 10^{9}$

Numerical results are shown in Fig. 4b and Fig. 5 in terms of damage patterns and load-displacement curves, respectively. As evidenced in Fig. 4b, the failure mode for both URM and FRP is characterized by the opening of the masonry joint between the first and second rows of blocks from the bottom (being the first row of block

clamped to the guided support), with crushing in the compressed side. Particularly, the reinforced case shows the debonding and consequent slipping of the four FRP strips form the substrate of the lowest blocks (green colour), while they remain bonded to the substrate in the rest of the structure (pink colour), Fig. 4b. This aspect has also been observed experimentally, as shown in Fig. 4c where the experimental failure of the FRP-masonry bond in the lowest block is highlighted [58].

Concerning the load-displacement curves of Fig. 5, an overall good agreement between the experimental ("exp") and the numerical ("num") outcomes can be observed. Particularly, the fact that the initial stiffness of the global response is not influenced by the presence of reinforcement, experimentally observed in [58], is also observed numerically in Fig. 5. Then, the numerical curves (both URM and FRP, with a gain in the FRP case of about the 50% of the horizontal force peak with respect to URM) fit rather well the nonlinear experimental responses until a horizontal displacement around 35 mm. At this point, the experimental tests have been stopped to avoid ruining the instrumentation, while the numerical responses have been simulated until full collapse. Indeed, significant softening is observed after 40 mm for FRP and after 25 mm for URM until a displacement around 75 mm, where the horizontal force goes to zero for both cases.

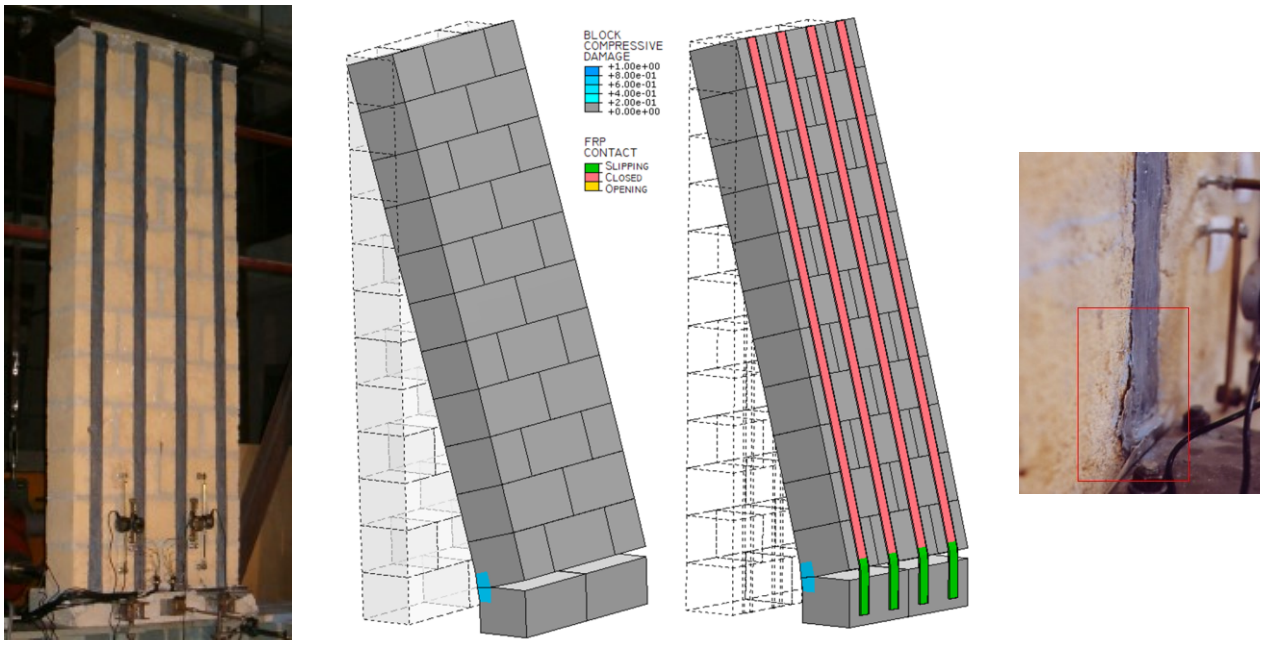

(a) (b) (c)

Fig. 4 – Out-of-plane loaded benchmark: (a) experimental specimen (from [58]), (b) numerical damage patterns with enlarged deformations for unreinforced (left) and reinforced (right) masonry walls, and (c) experimental failure of the FRP-masonry bond in the lowest block (from [58]).

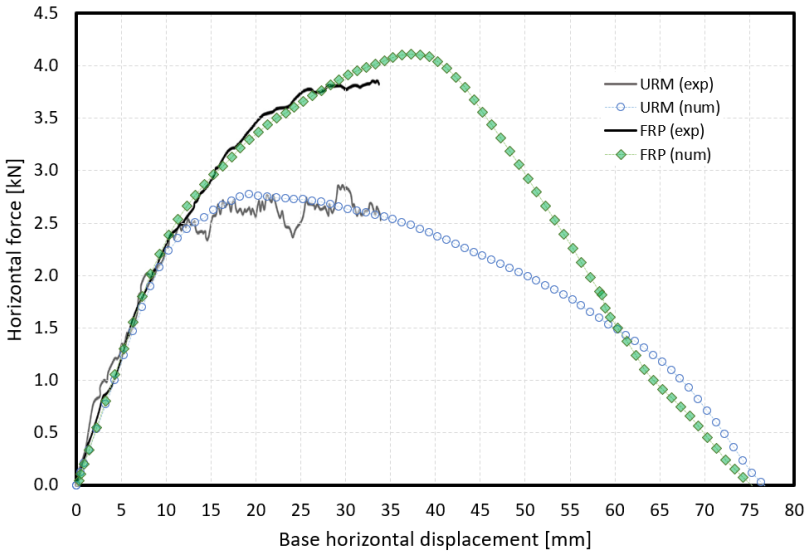

Fig. 5 – FRP-strengthened and URM out-of-plane benchmark: experimental-numerical comparison of load-displacement curves.

4.2 In-plane

The experimental tests performed by Milani et al. [45] are used as refence to check the potentialities of the modelling strategy in the analysis of FRP-strengthened masonry panels in-plane loaded. This choice is also motivated by the fact that these tests have been used in several scientific works [59, 60, 50, 61, 43] to validate numerical models and mechanical properties settings are available.

The experimental campaign discussed in [45] utilized 1:4-scale panels. Particularly, $0.29 \times 0.27 \times 0.03$ m CFRP-strengthened masonry panels (Fig. 6) were adopted in [45]. Small clay bricks ($0.056 \times 0.015 \times 0.030$ m) where used and bonded with cement-lime mortar. Following the acronyms used in [61], Pan_A was the URM wall, whereas Pan_A1 and Pan_A2 were strengthened with different arrangements of CFRP strips (width 12.5 mm, thickness 0.2 mm) on both sides of the wall, i.e. a single horizontal strip for Pan_A1 and two symmetrical diagonal strips for Pan_A2, see Fig. 6. The Young's modulus of the FRP strips was 160 GPa. The walls were vertically loaded, and the vertical displacements were measured on top of the walls next to the load cell. More details on the experimental set-up can be found in [45]. The experimental curves obtained for Pan_A, Pan_A1, and Pan_A2 in [45] are collected in Fig. 7, together with the numerical curves obtained in [50, 59, 61] and the limit analysis results from [45]. The mechanical properties settings adopted in [43, 50, 59, 60, 61] have been used to set the properties for masonry joint, block and FRP-masonry interface are collected in Table 4. Each (full) block has been discretized with 36 solid 8-node hexahedral FEs with linear shape functions. A nonlinear static analysis framework with geometric nonlinearity and imposed vertical displacements at the wall top has been conceived.

(a) (b) (c)

Fig. 6 – FRP-strengthened in-plane benchmark: experimental crack pattern for (a) Pan_A, (b) Pan_A1, and (c) Pan_A2.

Table 4. FRP-strengthened in-plane benchmark: mechanical parameters utilized in the numerical simulations.

Masonry joint mechanical properties (contact)		
Tensile cohesion	f_t [MPa]	0.2
Ultimate displacement of tensile cohesion	u_k [m]	$2 \cdot 10^{-4}$
Normal cohesive stiffness	K_{nn} [N/m^3]	$15 \cdot 10^{9}$
Shear cohesion	c [MPa]	0.28
Ultimate displacement of shear cohesion	δ_k [m]	$2 \cdot 10^{-4}$
Friction coefficient	$\tan \phi$ [\]	0.47
Tangential cohesive stiffness	K_{ss} [N/m^3]	$1.5 \cdot 10^{9}$
Masonry block mechanical properties (continuum)		
Young's modulus	E^B [MPa]	1785
Poisson's ratio	ν^B [\]	0.2
Tensile strength	f_t^B [MPa]	2.0
Fracture energy in tension	G_t^B [N/m]	$1 \cdot 10^{3}$
Compressive strength	f_c^B [MPa]	7.5
Fracture energy in compression	G_c^B [N/m]	$10 \cdot 10^{3}$
FRP-masonry interface mechanical properties (contact)		
Shear cohesion	f_s^{FRP} [MPa]	2
Fracture energy Mode II	G_{II}^{FRP} [N/m]	420
Shear cohesive stiffness	K_{ss}^{FRP} [N/m^3]	$7 \cdot 10^{9}$

Numerical results obtained with the numerical modelling strategy proposed herein are shown in Fig. 7, in terms of load-displacement curves (where they are compared with experimental and other numerical curves), and in Fig. 8, in terms of damage contour plots. Concerning the unreinforced case (Pan_A, Fig. 7a), the model proposed herein ("BBM") shows a load-displacement response in good agreement in terms of peak load, stiffness, and softening with the existing numerical approaches and the experimental results, even though these latter appear rather scattered. The damage contour plots obtained for Pan_A are shown in Fig. 8 (first row), in terms of vertical displacement, block tensile damage, and block compressive damage contour plots. No significant compressive damage appears, while the tensile damage is rather widespread in the blocks, suggesting their cracking, mainly for bending, and the formation of two diagonal struts in the masonry panel, allowing the load transfer from the point of application to the two supports (Fig. 8).

Concerning the reinforced panel Pan_A1 (Fig. 7b), two numerical configurations are compared with the existing experimental/numerical curves. On the one hand, the case "BBM FRP strips" implements the FRP-masonry interface model described Section 3.2, i.e. allowing debonding, with the mechanical parameters shown in Table 4. On the other hand, the case "BBM FRP strips perf. adh." adopts the hypothesis of perfect adhesion between FRP and the masonry substrate, without considering failure in the FRP-masonry interface. It has to be pointed out that the case of perfect adhesion represents a purely theoretical condition in which the FRP-masonry bond shear-slip behaviour is conceived as linear elastic, i.e. without the possibility of bond failure. Accordingly, this condition has no physical meaning and is merely used to facilitate the results discussion. As can be noted in Fig. 7b, the two curves are perfectly superimposed until the curve "BBM FRP strips" shows a sudden drop of the load, i.e. when the FRP-masonry bond fails. Conversely, the curve "BBM FRP strips perf. adh." keeps the load (that even increases) for more than 0.5 mm before showing a load drop. By inspecting the damage contour plots (Fig. 8, second and third rows), the different failure mode of the two configurations can be clearly noted. Indeed, the case which allows debonding shows the failure of the FRP-masonry bond in the two extremities together with a widespread tensile damage in the blocks and a significant compressive damage in the blocks just in proximity of the bottom supports. The combination of tensile and compressive damage in these blocks suggests their shear failure, that can also be noted by the enhanced deformed shape (Fig. 8, second row). Conversely, the case with perfect adhesion shows mainly the shear failure of the blocks in the top-central part of the wall (Fig. 8, third row), being not possible the debonding of the FRP strips. By comparing the load-displacement curves with the reference ones, it appears a rather good agreement in terms of peak load, stiffness, and softening, even though the case which allows debonding shows a slightly lower peak load and slightly earlier load drop than other numerical approaches, although comparable with the

curve “Experimental 2”, while the case “BBM FRP strips perf. adh.” effectively overestimate the wall capacity. Therefore, the block-based model with a cohesive FRP-masonry interface appears capable of accurately account for FRP-from-masonry debonding.

Concerning the reinforced panel Pan_A2 (Fig. 7c), three numerical configurations are compared with the existing experimental/numerical curves. Firstly, the case “BBM FRP short strips” considers shorter FRP strips than the actual case, i.e. the diagonal strips are interrupted when they run into each other. This simplistic assumption has been made in the works [59, 61, 45] given that the meshes that have been adopted there were compatible and the two strips shared a common node. Secondly, the case “BBM FRP strips” considers the real geometry of the FRP reinforcement, while, thirdly, the case “BBM FRP strips perf. adh.” does not implement any failure in the FRP-masonry interface. As can be noted in Fig. 7c and Fig. 8 (last three rows), the three configurations show significant differences. Indeed, a reduction of more than 30% in the peak load is observed when passing from the real geometry of the strip to the shorter ones (being the mesh non-compatible between the two strips in this case). Basically, the case “BBM FRP strips” shows a good agreement with the experimental curves and the other numerical responses, although it shows a slightly earlier load drop. Also in this case, the configurations with and without debonding of the FRP-masonry interface are substantially superimposed until the FRP-from-masonry debonding occurs in the second case. It is worth to note that, although the case “BBM FRP short strips” has shorter strips, its stiffness appears slightly greater than the other cases, being completely different the resistant mechanism between these cases (e.g. compare the last two rows in Fig. 8). Indeed, the case with short strips shows the formation of a vertical crack in the middle of the wall, together with shear failure of the blocks just in proximity of the supports in the bottom, whereas the case with perfect adhesion is mainly characterized by the sole shear failure of these blocks (Fig. 8). On the contrary, the case “BBM FRP strips” initially shows mostly the same behaviour of the case with perfect adhesion (i.e. when the strips are fully bonded to the substrate), while when debonding occurs at the lowest extremity of one strip (per each side) the sudden formation of the vertical crack occurs, in a similar way to the short strip case (Fig. 8), and to the actual crack pattern (Fig. 6c). Hence, the potential of this modelling strategy to properly consider structural details (which can have a significant impact on the structural response, e.g. see Fig. 7c) in FRP-strengthened masonry structures appears significant and appealing.

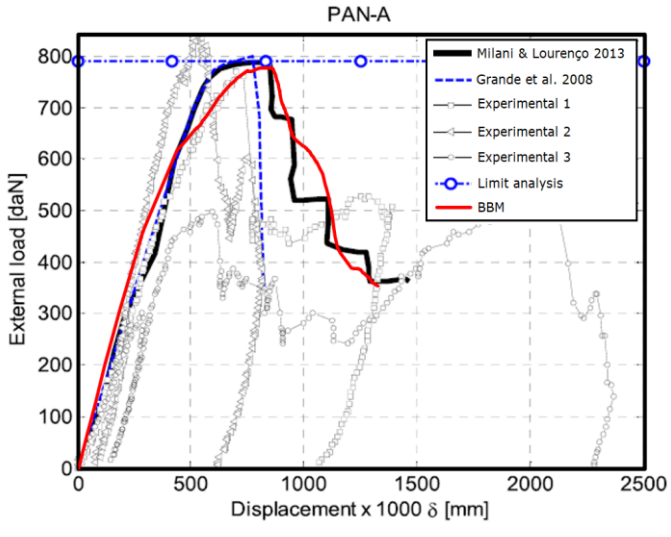

(a)

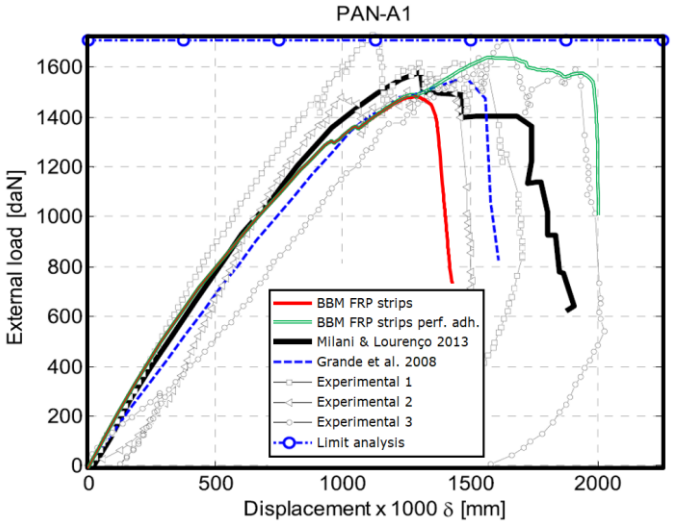

(b)

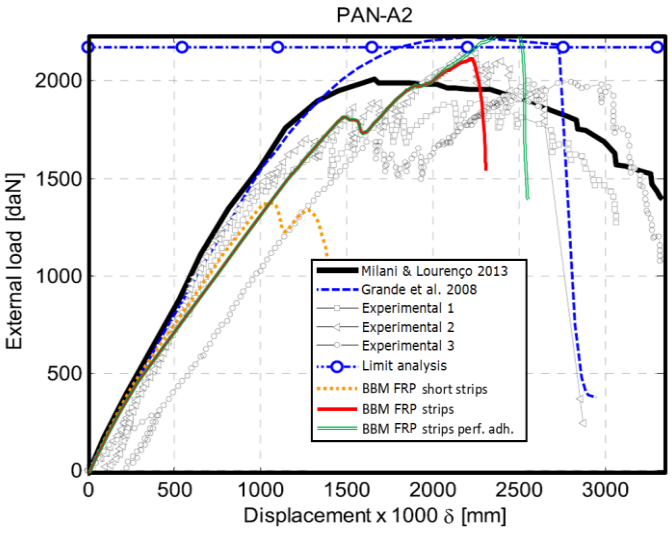

(c)

Fig. 7 – FRP-strengthened in-plane benchmark: comparison of load-displacement curves for (a)Pan_A, (b) Pan_A1, and (c) Pan_A2.

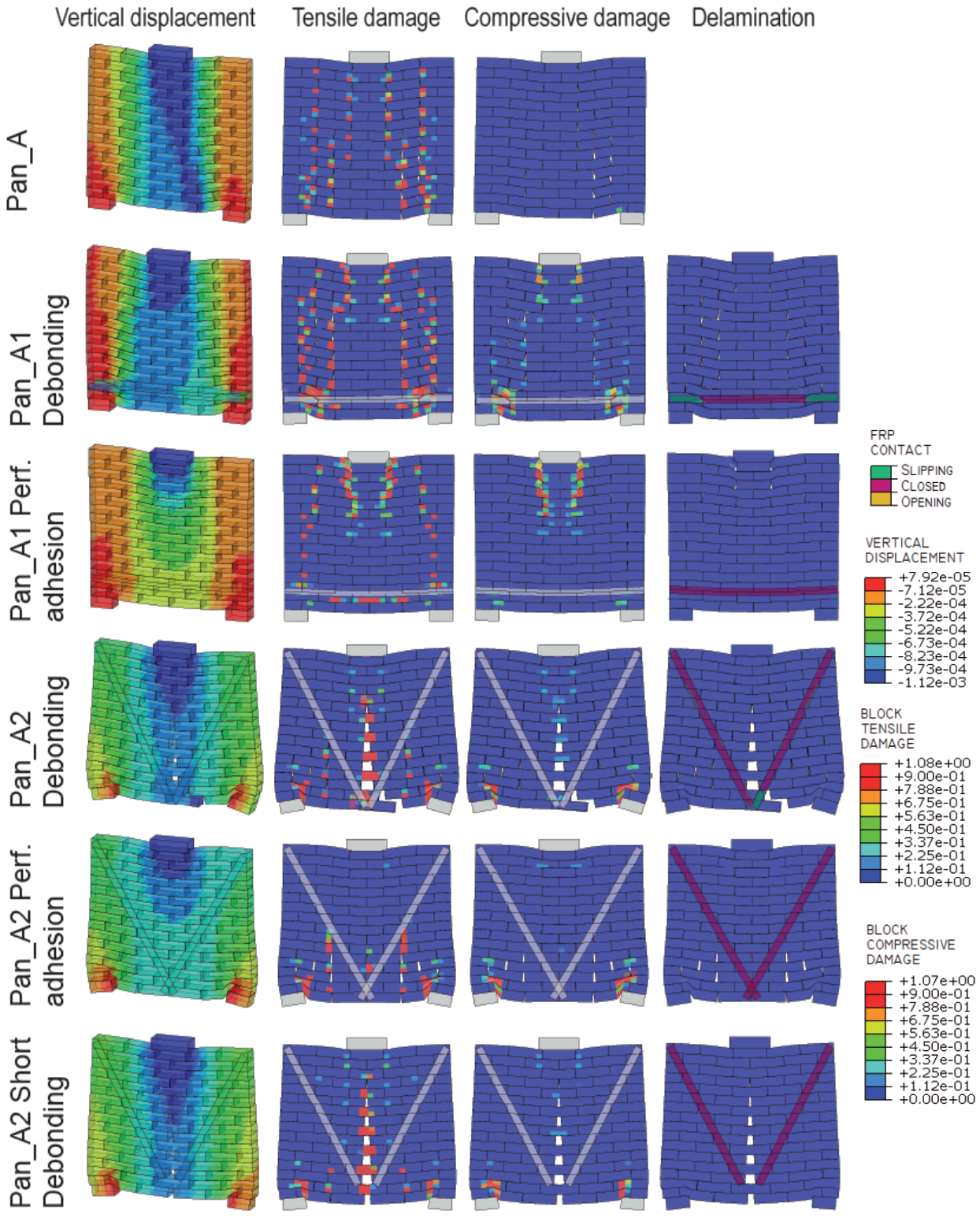

Fig. 8 – FRP-strengthened in-plane benchmarks: damage contour plots.

5 Loss of performance in FRP strengthening systems bonded to masonry structures due to environmental degradation

The objective of this paper is to evaluate the environmentally-induced loss of performance in FRP strengthening systems bonded to masonry structures. On the one hand, the degradation of the material properties in the numerical model is deduced from small scale experimental tests (e.g. single-lap shear tests). On the other hand, the environmentally-induced loss of performance is evaluated in FRP strengthening systems bonded to full-scale masonry structures. The flowchart sketched in Fig. 9 represents the core of this study.

Firstly, numerical analyses on the FRP-strengthened masonry structure to be investigated are performed with non-degraded material properties to predict the structural response at design conditions. These numerical analyses can be performed with the modelling strategy presented in Section 3, which demonstrated to be rather accurate and reliable (Section 4).

Then, degraded material properties can be deduced from experimental campaigns on material ageing (e.g. the ones described in Section 2), i.e. from experimental campaigns which investigated environmental degradation in FRP-strengthened masonry, and are adopted in the same numerical analysis framework to predict the structural response at degraded conditions. Therefore, the environmentally-induced loss of performance in FRP strengthening systems bonded to masonry structures is deduced by comparing the structural response at degraded conditions with the one at design conditions.

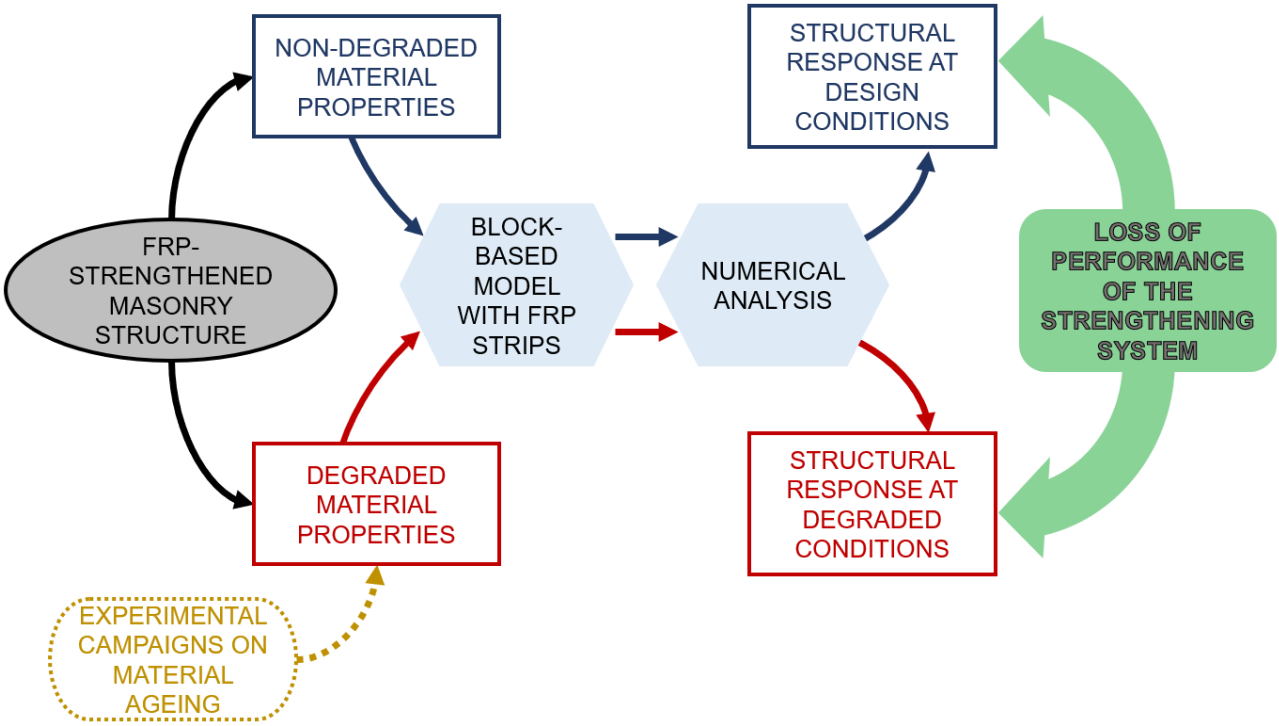

Fig. 9 – Flowchart followed to evaluate the loss of performance in FRP strengthening systems bonded to masonry structures due to environmental degradation

In the following, the assessment of performance loss due to environmental degradation is shown for some examples of FRP-strengthened masonry structures. Particularly, the examples of out-of-plane and in-plane loaded walls and a full-scale house are shown and discussed in Sections 5.1, 5.2, and 5.3, respectively. It has to be pointed out that all the numerical results presented in this section are original, exception made for the unreinforced (URM) case of the full-scale house (Section 5.3) which has been already presented in [44], where the model for unreinforced masonry has been validated.

Degraded material properties related to FRP and FRP-masonry bond have been only considered in this study, while masonry properties have been kept unchanged. This choice has been made given that this paper aims to assess the loss of performance of FRP strengthening systems bonded to masonry structures due to

environmental degradation. However, the approach proposed herein can be easily extended to account for environmentally-induced degradation in the masonry material (see for example [62, 63, 64]), altering the masonry mechanical properties analogously to what proposed for FRP strengthening systems.

Concerning the degraded material properties, reference to Section 2 is made to define their deterioration. Particularly, by inspecting Table 1 and having in mind to check the worst case scenario for the durability of FRP-strengthening systems bonded to masonry, the percentage degradation values collected in (7) are assumed. Basically, the outcomes obtained in the experimental campaigns presented in [37, 36, 38] have been considered.

$$\Delta E^{FRP} = -38\%, \qquad \Delta f_s^{FRP} = -45\%, \qquad \Delta G_{II}^{FRP} = -60\%, \qquad \Delta K_{ss}^{FRP} = -80\%. \qquad (7)$$

The effects of the percentage degradation values collected in (7) on the FRP-masonry interface contact behaviour (Fig. 3) are shown in Fig. 10, where the single effect of the degradation of each quantity in (7) (except for ΔE^{FRP}) is also displayed.

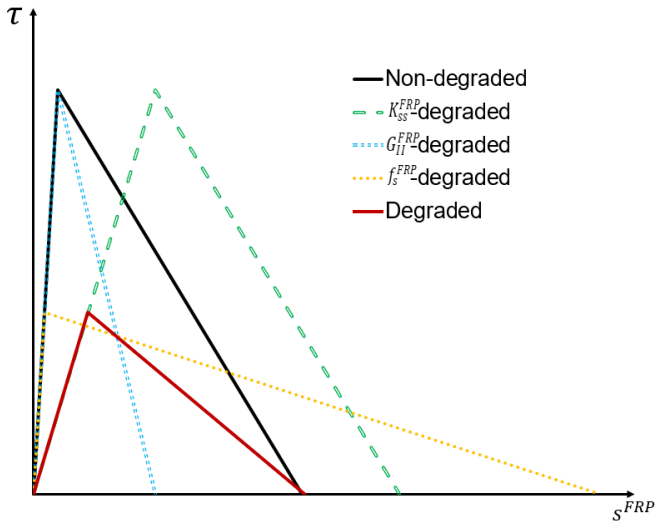

Fig. 10 – Effects of environmental degradation on the FRP-masonry interface shear contact behaviour.

5.1 Out-of-plane loaded wall

The same benchmark presented in Section 4.1 has been used herein to show the loss of performance of FRP strengthening systems applied to an out-of-plane loaded masonry wall due to environmental degradation. The load-displacement curves shown in Fig. 11 have been obtained by degrading the material properties of Table 3 with the percentages of deterioration shown in (7). In particular, the curves "URM" and "FRP" are the same numerical curves shown in Fig. 5, the curve "Perfect adhesion" is obtained by neglecting the failure at the FRP-masonry bond, the curve "FRP-DEGRADED" is obtained with the degradation of all the properties shown in (7), while the other curves highlight the single contribution of the degradation of each material property shown in (7). Exception made for the "Perfect adhesion" case (without physical meaning) which showed tensile cracking in the blocks glued to the guided support in the bottom, all the other cases experienced the same failure mode depicted in Fig. 4, i.e. debonding of the FRP strips from the substrate of the lowest blocks.

As can be noted in Fig. 11, the loss of performance of the FRP reinforcement appears considerable (compare the curve "FRP" with the curve "FRP-DEGRADED"). Indeed, if the non-degraded reinforced case shows a benefit in terms of peak load around the 48% with respect to the unreinforced case, the benefit of the degraded reinforced case is limited to about 18%, showing a significant loss of performance of the FRP strengthening system of about 30%.

By inspecting in Fig. 11 the single contribution of the degradation of each material property shown in (7), it appears that:

- the degradation of the FRP-masonry bond Mode II fracture energy G_{II}^{FRP} affects, as expected, the post-peak behaviour which becomes significantly steeper, i.e. the load drop is more sudden;
- the degradation of the FRP Young's modulus E^{FRP} slightly affects the structural response;
- the degradation of the FRP-masonry bond strength f_s^{FRP} significantly affects the peak load;
- the degradation of the FRP-masonry bond stiffness K_{ss}^{FRP} significantly affects both the peak load (which is comparable with the one obtained with the degradation of f_s^{FRP}) and the stiffness after masonry cracking, i.e. with displacements greater than about 10 mm.

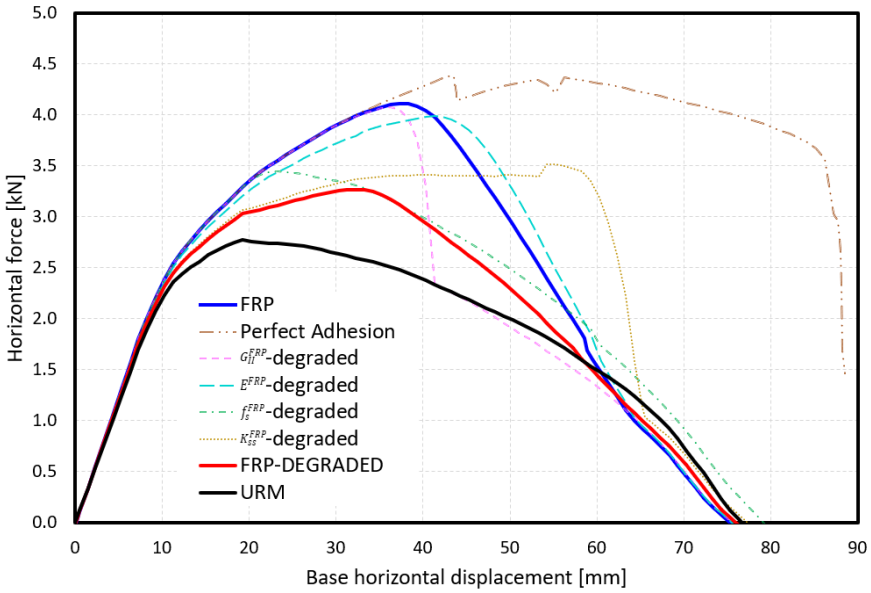

Fig. 11 – Effects of environmental degradation on the structural performance of an out-of-plane loaded wall: impact of the various material properties.

5.2 In-plane loaded wall

The benchmark presented in Section 4.1 has been used herein also to show the environmentally-induced loss of performance of FRP strengthening systems applied to an in-plane loaded masonry wall. This benchmark has been preferred to the one used in Section 4.2, i.e. the one tested in [45]. Indeed, it has to be pointed out that the benchmark in Section 4.1 is a 1:1-scale wall, whereas the benchmark in Section 4.2 is a 1:4-scale wall. From a physical point of view, it appears reasonable to suppose that environmental degradation can have a sort of "scale effect", i.e. for the same environmental action, the impact in terms of degradation on a narrow FRP strip (e.g. environmental degradation on a single-lap shear test with a 5 mm width FRP strip) will be, in general, different with respect to a larger one (e.g. environmental degradation on a single-lap shear test with a 50 mm width FRP strip), even though no experimental outcomes are available to quantify this aspect. From a numerical point of view, the degraded properties of the FRP-masonry bond are deduced from single-lap shear tests and accounted for in a simplified manner. Therefore, the potential scale effects of degradation could be simply introduced in the model as input (i.e. in the FRP-masonry stress-slip bond behaviour as function, for instance, of the strip width), once experimental outcomes will supply sufficient data on this purpose. So, examples with the same (real) scale have been preferred in this section.

The boundary conditions have been changed on the model presented in Section 4.1 to simulate an in-plane loaded wall. Particularly, clamped boundary conditions have been assumed at the base of the wall, while horizontal displacement have been imposed to the top nodes of the wall, fixing the out-of-plane displacements. The initial vertical compression applied to the wall has been reduced, simply by the ratio between thickness and width of the wall, to not induce premature crushing failure in the wall. Therefore, a constant 22.7 kN vertical force is applied to generate vertical compression in the masonry panel. Beyond the unreinforced wall "URM" used as reference, two strengthening configurations have been considered, i.e. reinforcement on one side of the wall only "FRP-SINGLE", and reinforcement on both sides of the wall "FRP-DOUBLE" (Fig. 12), assuming the same reinforcement arrangement utilized in Section 4.1.

Numerical results are shown in Fig. 12 and Fig. 13 in terms of damage patterns and load-displacement curves, respectively. As evidenced in Fig. 12a, the failure mode for all cases (also in the degraded ones) is characterized by the opening of the masonry joint between the first and second rows of blocks from the bottom (being the first row of block clamped to the base), with crushing in the compressed side. Particularly, both FRP-SINGLE and FRP-DOUBLE show the debonding and consequent slipping of three FRP strips form the substrate of the lowest blocks (green colour), while the strips closer to the compressed side rather clearly show buckling, i.e. local detachment of the strips from the masonry substrate in the normal direction ("opening"), Fig. 12a. This phenomenon appears quite common in experimental observations when FRP strips are bonded to a compressed masonry substrate, see for example Fig. 12b.

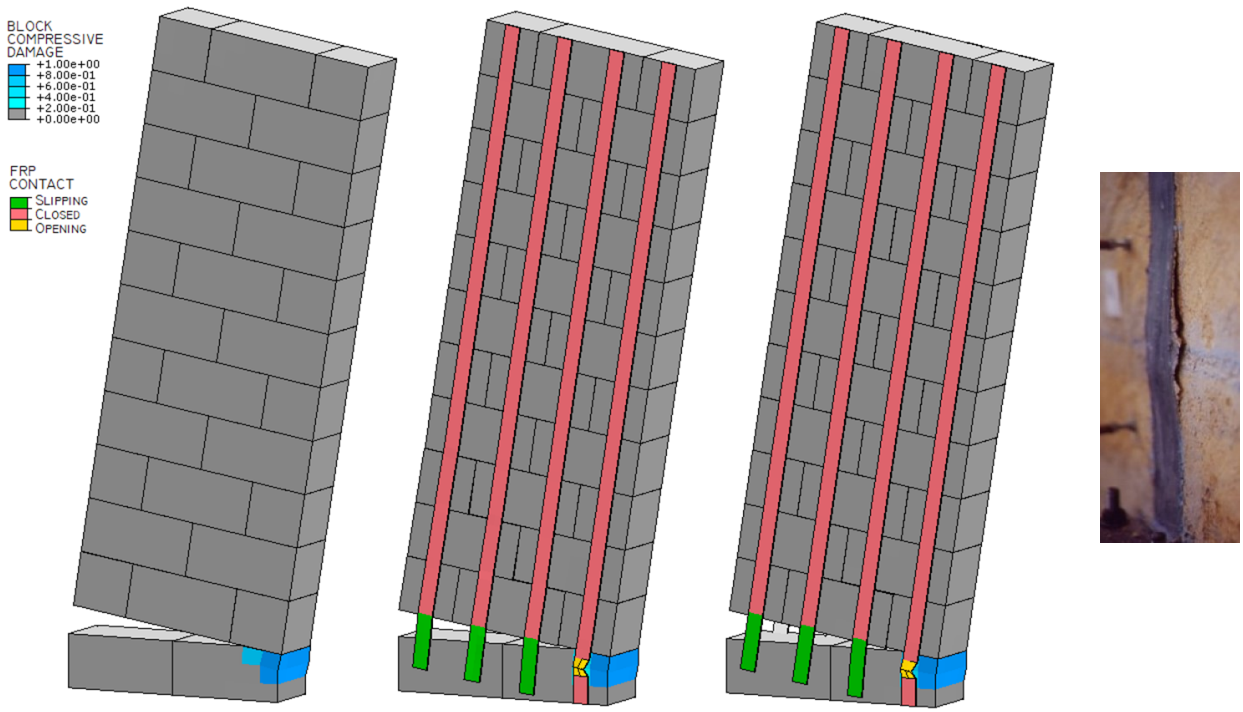

(a) (b)

Fig. 12 – In-plane loaded FRP-strengthened masonry wall used for evaluating the environmentally-induced loss of performance of strengthening systems: (a) URM (left), FRP-SINGLE (middle), and FRP-DOUBLE (right) cases, (b) example of FRP strip buckling (from [58]).

The degraded load-displacement curves shown in Fig. 13 have been obtained by degrading the material properties of Table 3 with the percentages of deterioration shown in (7). In this case, the loss of performance of the FRP reinforcement appears even more significant than the out-of-plane loaded case. Indeed, the benefit of the "FRP-SINGLE" case with respect to the unreinforced case (around the 28% of peak load), is totally wasted by the "FRP-SINGLE-DEGRADED" case, which just shows base shear values slightly greater than URM in the first part of the post-peak response. The performance loss in the "FRP-DOUBLE" case is even more considerable, given that the benefit of the strengthening systems goes from the 90% for the non-degraded case to the 18% for the degraded case, with a 72% global performance loss of the reinforcement. It is worth to note in Fig. 13 that the curve "FRP-DOUBLE-DEGRADED" remains lower than the "FRP-SINGLE" curve, suggesting that a degraded reinforcement at the two faces of the wall can show lower performances than a non-degraded wall reinforced just on one side.

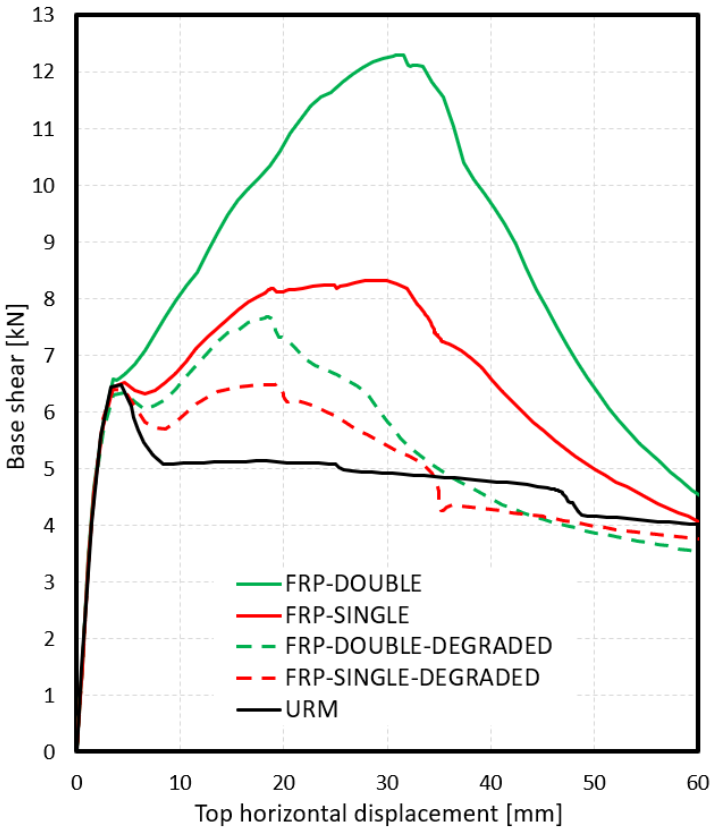

Fig. 13 – Environmentally-induced performance loss for an in-plane loaded FRP-strengthened masonry wall.

5.3 Full-scale house

In this section, the environmentally-induced loss of performance of an hypothetical FRP strengthening system applied to a two-storey full-scale masonry terraced house is presented (Fig. 14). The house model, which has been validated in [44] for the cyclic regime, reproduces the experimental set-up developed in [65, 66]. Masonry mechanical parameters are collected in [44], where they have been calibrated through a multi-scale experimental testing framework [67]. Also, the mesh and the boundary conditions imposed to the model are the same of the ones adopted in [44]. The strengthening systems supposed in Fig. 14 (where half structure is shown) consists of 7 FRP strips 2.8 m long externally bonded to the piers (i.e. 5 strips on the larger pier and 2 strips on the smaller pier). Basically, the piers are reinforced only in the external side between the base and the first floor. For simplicity, the same properties of the FRP strips utilized in Section 4.1 are assumed, using 100 mm FRP strips thickness. The strengthening systems has to be considered symmetric also in the non-displayed half structure (Fig. 14).

It has to be pointed out that the conceptualization of this strengthening system did not follow any consolidated design rule, and it has not to be considered as an optimized and fully efficient reinforcement. Indeed, it only serves as example to show the potential environmentally-induced loss of performance of the FRP strengthening system in a full-scale masonry structure. Particularly, the degradation of the FRP strips is supposed only in the bottom part of the reinforcements (Fig. 14), i.e. from the base up to 0.72 m, to make the environmental degradation pattern more realistic. Indeed, it is expected that rising damp mainly interests the lower portion of the structure, typically within the first meter from the bottom, as observed in [68] (see the photo in Fig. 14). Thereby, given that the material properties degradation observed in [36, 38] concerned almost full-saturated specimens, the hypothesis of partial degradation depicted in Fig. 14 appears reasonable.

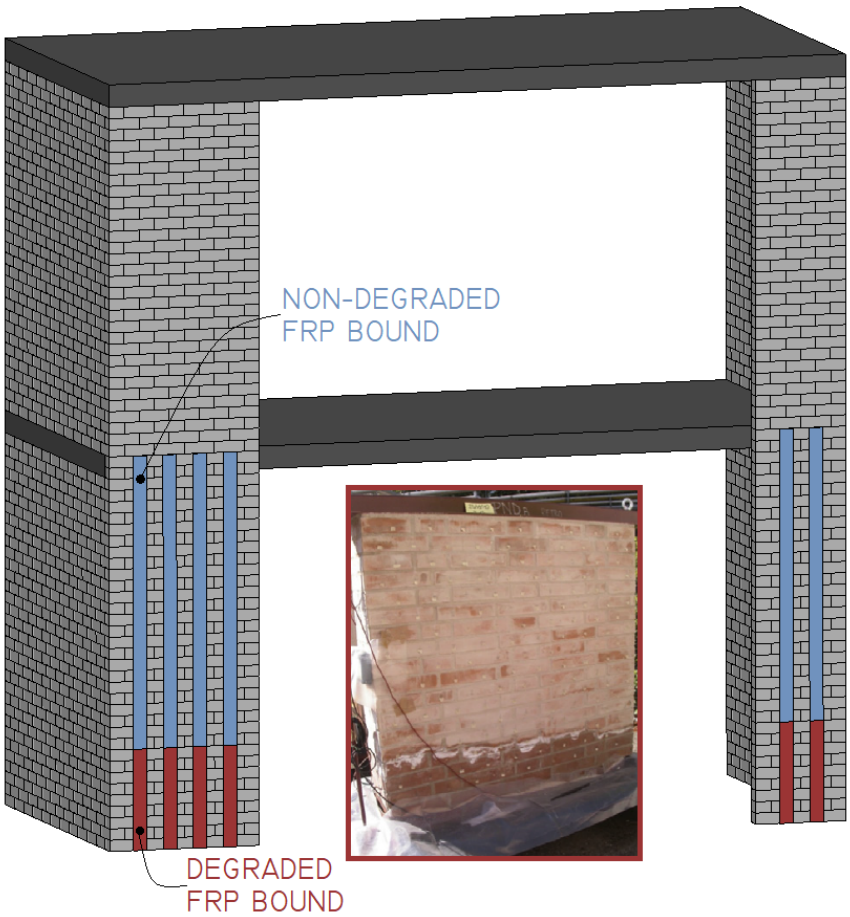

Fig. 14 – Full-scale masonry house (from [44]) strengthened with FRP strips. The degraded reinforcement portions are highlighted in red. The photo (from [68]) shows an example of moisture distribution in a masonry wall.

Numerical results in terms of load-displacement curves (monotonic pushover analysis), deformed shapes at 50 mm top displacement and damage contour plots at the end of the analysis are shown in Fig. 15, Fig. 16, and Fig. 17, respectively. As can be noted in Fig. 15, the loss of performance of the FRP reinforcement appears significant also in this case, despite the partial and limited strengthening system and the partial degradation of the FRP strips, see Fig. 14 (compare the curve "FRP" with the curve "FRP-DEGRADED" in Fig. 15). On the one hand, the non-degraded reinforced "FRP" case shows a benefit in terms of peak load around the 30% with respect to the unreinforced case "URM" (from [44]), the benefit of the degraded reinforced case is limited to about 8%, showing a 22% loss of performance of the FRP strengthening system due to environmental degradation. Additionally, a significant reduction of energy dissipated by the structure due to environmental degradation can be deduced from Fig. 15.

By comparing the deformed shapes (enlarged) between unreinforced (Fig. 16a from [44]) and reinforced (Fig. 16b) full-scale masonry house at a 50 mm top horizontal displacement, it can be noted that, although the FRP strips limit the crack opening in the smaller pier and the shear crack propagation in the larger pier, significant cracking appears in the out-of-plane loaded walls and between the top floor and the bearing walls. The damage contour plot in Fig. 17 shows the compressive damage in the masonry blocks (substantially in the bottom right of the larger pier and in the top left of the smaller pier), and the failure mode of the FRP-masonry bond. Particularly, both the strips of the smaller pier show the debonding from the lowest blocks, and this pier reaches a failure similar to the one shown in Fig. 16a. Conversely, in the larger pier the two strips on the left showed debonding from the lowest blocks, the one on the right showed opening in the normal direction (given that it was close to the compressed side), while the second strip from the right did not show any failure, leading to a failure mode of the pier considerably different from the one shown in Fig. 16a, i.e. a pseudo-flexural failure with rotation in the lowest masonry joint (Fig. 17) instead of a more shear-like failure (Fig. 16a).

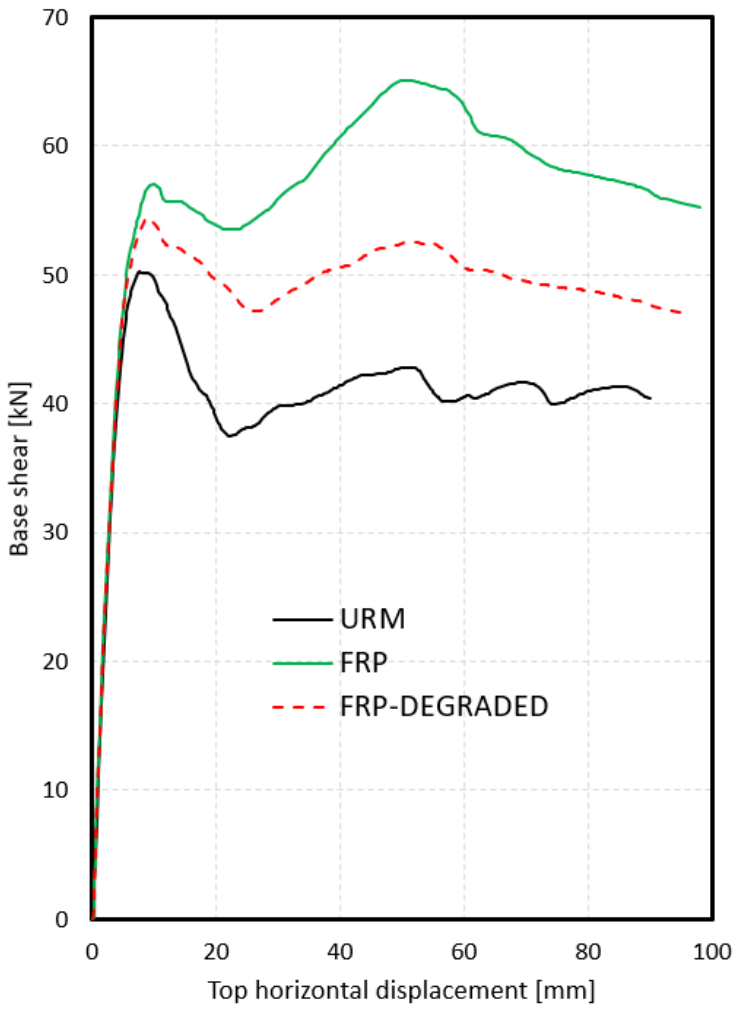

Fig. 15 – Environmentally-induced performance loss for an FRP-strengthened full-scale masonry house.

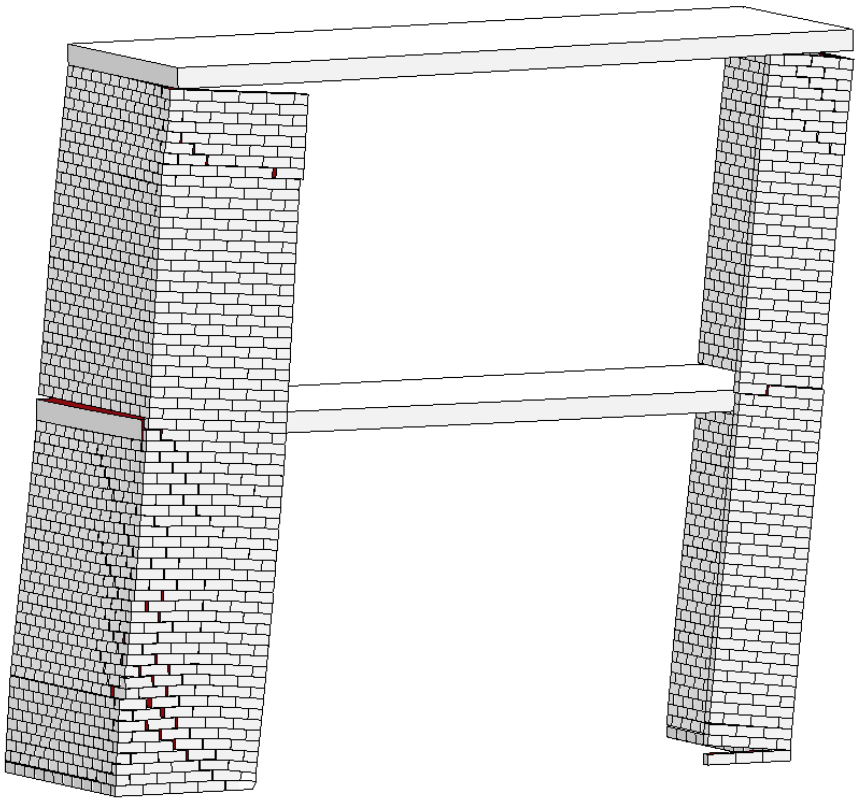

(a)

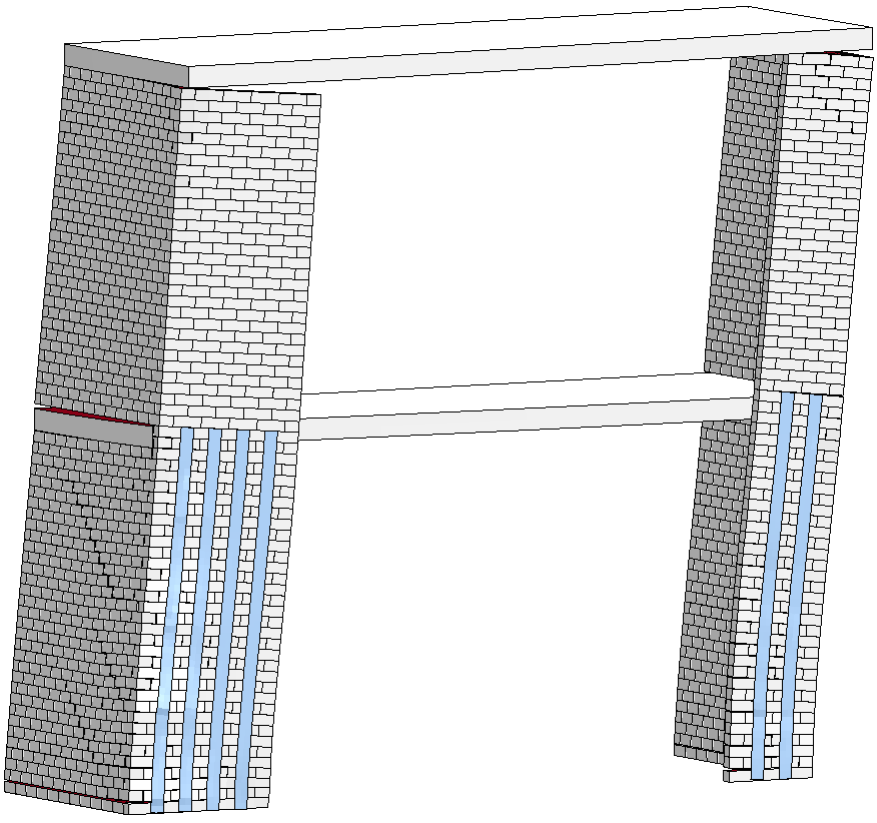

(b)

Fig. 16 – Comparison of deformed shapes (enlarged) between (a) unreinforced (from [44]) and (b) reinforced full-scale masonry house at a 50 mm top horizontal displacement.

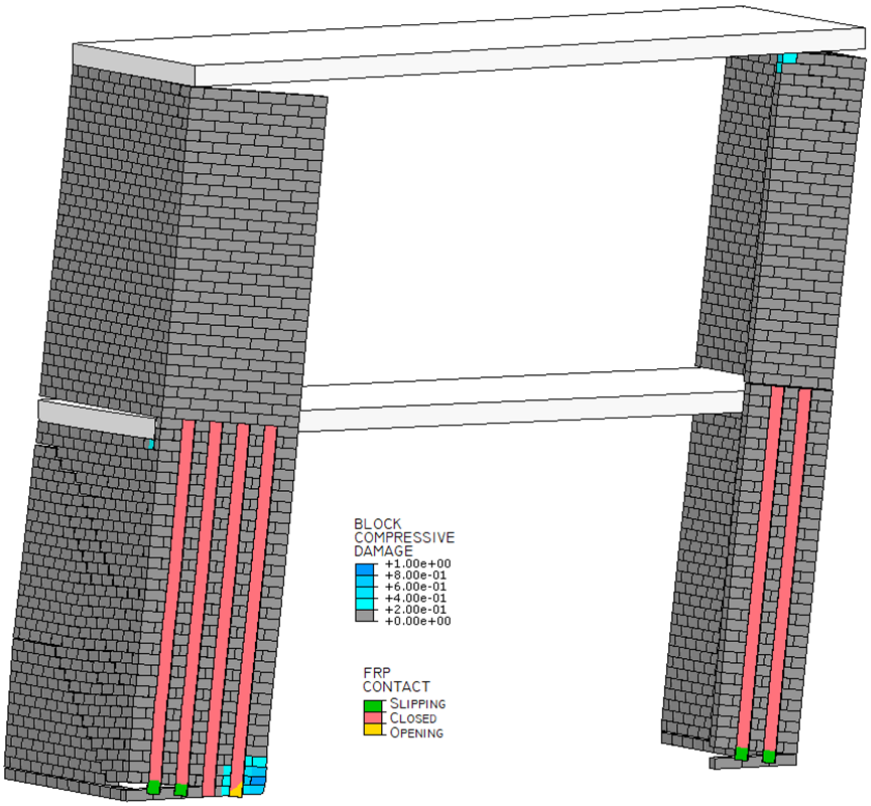

Fig. 17 – Damage contour plot for the reinforced full-scale masonry house at the end of the simulation.

6 Conclusions

In this paper, the environmentally-induced loss of performance in FRP strengthening systems bonded to masonry structures has been numerically investigated. A damaging block-based modelling strategy, lately developed by the authors, has been used to model masonry, whereas the bond of FRP strips to masonry blocks have been idealized through a contact-based formulation with cohesion. This approach has been validated against in- and out-of-plane loaded FRP-strengthened masonry wall benchmarks, showing good results and appealing potentialities of the modelling strategy.

The assessment of performance loss due to environmental degradation has been shown for some examples of FRP-strengthened masonry structures, i.e. out-of-plane and in-plane loaded walls and a full-scale house. Numerical analyses have been performed with non-degraded material properties to predict the structural response at design conditions. Then, degraded material properties have been deduced from accelerated ageing laboratory tests which investigated environmental degradation in FRP-strengthened masonry. These degraded properties have been adopted in the same numerical analysis framework to predict the structural response at degraded conditions.

Therefore, the environmentally-induced loss of performance in FRP strengthening systems bonded to masonry structures has been deduced by comparing the structural response at degraded conditions with the one at design conditions. As a result, the loss of performance in FRP-strengthened structures due to environmental degradation appeared considerable (around the 30%, 72%, and 22% in terms of peak load for the out-of-plane wall, “FRP-DOUBLE” in-plane wall and house, respectively), up to the total waste of the strengthening benefit (e.g. “FRP-SINGLE” in-plane wall). This aspect appears particularly strategic, as environmental degradation is expected to become even more significant in view of the future worsening of environmental actions according to climate change predictions.

ACKNOWLEDGEMENTS

Financial support by the Italian Ministry of Education, Universities and Research MIUR is gratefully acknowledged (PRIN2015 "Advanced mechanical modeling of new materials and structures for the solution of 2020 Horizon challenges" prot. 2015JW9NJT_018).

REFERENCES

[1] N. G. Shrive, "The use of fibre reinforced polymers to improve seismic resistance of masonry," *Construction and Building Materials,* vol. 20, no. 4, pp. 269-277, 2006.

[2] F. G. Carozzi, C. Poggi, E. Bertolesi and G. Milani, "Ancient masonry arches and vaults strengthened with TRM, SRG and FRP composites: Experimental evaluation," *Composite Structures,* vol. 187, pp. 466-480, 2018.

[3] N. Reboul, Z. Mesticou, A. S. Larbi and E. Ferrier, "Experimental study of the in-plane cyclic behaviour of masonry walls strengthened by composite materials," *Construction and Building Materials,* no. 164, 70-83.

[4] T. C. Triantafillou, "Strengthening of masonry structures using epoxy-bonded FRP laminates," *Journal of composites for construction,* vol. 2, no. 2, pp. 96-104, 1998.

[5] J. Vaculik, P. Visintin, N. G. Burton, M. C. Griffith and R. Seracino, "State-of-the-art review and future research directions for FRP-to-masonry bond research: Test methods and techniques for extraction of bond-slip behaviour," *Construction and Building Materials,* vol. 183, pp. 325-345, 2018.

[6] M. R. Ehsani, H. Saadatmanesh and A. Al-Saidy, "Shear behavior of URM retrofitted with FRP overlays," *Journal of composites for construction,* vol. 1, no. 1, pp. 17-25, 1997.

[7] M. R. Valluzzi, D. Tinazzi and C. Modena, "Shear behavior of masonry panels strengthened by FRP laminates," *Construction and Building materials,* vol. 16, no. 7, pp. 409-416, 2002.

[8] C. Carloni and K. V. Subramaniam, "FRP-masonry debonding: numerical and experimental study of the role of mortar joints," *Journal of composites for construction,* vol. 16, no. 5, pp. 581-589, 2012.

[9] D. V. Oliveira, I. Basilio and P. B. Lourenço, "Experimental behavior of FRP strengthened masonry arches," *Journal of Composites for Construction,* vol. 14, no. 3, pp. 312-322, 2010.

[10] C. Faella, G. Camorani, E. Martinelli, S. O. Paciello and F. Perri, "Bond behaviour of FRP strips glued on masonry: experimental investigation and empirical formulation," *Construction and Building Materials,* vol. 31, pp. 353-363, 2012.

[11] Z. Al-Jaberi, J. J. Myers and M. A. ElGawady, "Pseudo-static cyclic loading comparison of reinforced masonry walls strengthened with FRCM or NSM FRP," *Construction and Building Materials,* vol. 167, pp. 482-495, 2018.

[12] I. Basilio, R. Fedele, P. B. Lourenço and G. Milani, "Assessment of curved FRP-reinforced masonry prisms: experiments and modeling," *Construction and Building Materials,* vol. 51, pp. 492-505, 2014.

[13] M. Corradi, A. Borri and A. Vignoli, "Strengthening techniques tested on masonry structures struck by the Umbria–Marche earthquake of 1997–1998," *Construction and Building Materials,* vol. 16, no. 4, pp. 229-239, 2002.

[14] C. Mazzotti, B. Ferracuti and A. Bellini, "Experimental bond tests on masonry panels strengthened by FRP," *Composites Part B: Engineering,* vol. 80, pp. 223-237, 2015.

[15] G. de Felice, M. A. Aiello, A. Bellini, F. Ceroni, S. De Santis and E. Garbin, "Experimental characterization of composite-to-brick masonry shear bond," *Materials and Structures,* vol. 49, no. 7, pp. 2581-2596, 2016.

[16] P. Carrara, D. Ferretti and F. Freddi, "Debonding behavior of ancient masonry elements strengthened with CFRP sheets," *Composites Part B: Engineering,* vol. 45, no. 1, pp. 800-810, 2013.

[17] F. Ceroni, G. de Felice, E. Grande, M. Malena, C. Mazzotti and F. Murgo, "Analytical and numerical modeling of composite-to-brick bond," *Materials and structures,* vol. 47, no. 12, pp. 1987-2003, 2014.

[18] C. Carloni and F. Focacci, "FRP-masonry interfacial debonding: An energy balance approach to determine the influence of the mortar joints," *European Journal of Mechanics-A/Solids,* vol. 55, pp. 122-133, 2016.

[19] F. G. Carozzi, P. Colombi and C. Poggi, "Calibration of end-debonding strength model for FRP-reinforced masonry," *Composite Structures,* vol. 120, pp. 366-377, 2015.

[20] P. K. V. R. Padalu, Y. Singh and S. Das, "Out-of-plane flexural strengthening of URM wallettes using basalt fibre reinforced polymer composite," *Construction and Building Materials,* vol. 216, pp. 272-295, 2019.

[21] R. Luciano and E. Sacco, "Damage of masonry panels reinforced by FRP sheets," *International Journal of Solids and Structures,* vol. 35, no. 15, pp. 1723-1741, 1998.

[22] F. Freddi and E. Sacco, "An interphase model for the analysis of the masonry-FRP bond," *Composite Structures,* vol. 138, pp. 322-334, 2016.

[23] E. Bertolesi, G. Milani, M. Fagone, T. Rotunno and E. Grande, "Micro-mechanical FE numerical model for masonry curved pillars reinforced with FRP strips subjected to single lap shear tests," *Composite Structures,* vol. 201, pp. 916-931, 2018.

[24] E. Bertolesi, G. Milani and R. Fedele, "Fast and reliable non-linear heterogeneous FE approach for the analysis of FRP-reinforced masonry arches," *Composites Part B: Engineering,* vol. 88, pp. 189-200, 2016.

[25] E. Bertolesi, G. Milani, F. G. Carozzi and C. Poggi, "Ancient masonry arches and vaults strengthened with TRM, SRG and FRP composites: Numerical analyses," *Composite Structures,* vol. 187, pp. 385-402, 2018.

[26] E. Grande, M. Fagone, T. Rotunno, E. Bertolesi and G. Milani, "Modelling of the bond behaviour of curved masonry specimens strengthened by CFRP with anchor spikes," *Composites Part B: Engineering,* vol. 171, pp. 235-245, 2019.

[27] A. M. D'Altri, C. Carloni, S. de Miranda and G. Castellazzi, "Numerical modeling of FRP strips bonded to a masonry substrate," *Composite Structures,* vol. 200, pp. 420-433, 2018.

[28] F. Ceroni, M. Leone, V. Rizzo, A. Bellini and C. Mazzotti, "Influence of mortar joints on the behaviour of FRP materials bonded to different masonry substrates," *Engineering Structures,* vol. 153, pp. 550-568, 2017.

[29] S. de Miranda, A. M. D'Altri and G. Castellazzi, "Modeling environmental ageing in masonry strengthened with composites," *Engineering Structures,* vol. 201, p. 109773, 2019.

[30] C. Tedeschi, A. Kwiecień, M. R. Valluzzi, B. Zając, E. Garbin and L. Binda, "Effect of thermal ageing and salt decay on bond between FRP and masonry," *Materials and structures,* vol. 47, no. 12, pp. 2051-2065, 2014.

[31] C. Gentilini, E. Franzoni, M. Santandrea and C. Carloni, "Salt-Induced Deterioration on FRP-Brick Masonry Bond," in *Structural Analysis of Historical Constructions*, Springer, Cham, 2019, pp. 1914-1921.

[32] G. Cardani, M. R. Valluzzi, M. Panizza, P. Girardello and L. Binda, "Influence of salt crystallization on composites-to-masonry bond evaluated on site by pull-off tests," *Key Engineering Materials,* vol. 624, pp. 338-345, 2015.

[33] M. S. Sciolti, M. A. Aiello and M. Frigione, "Influence of water on bond behavior between CFRP sheet and natural calcareous stones," *Composites Part B: Engineering,* vol. 43, no. 8, pp. 3239-3250, 2012.

[34] M. S. Sciolti, M. A. Aiello and M. Frigione, "Effect of thermo-hygrometric exposure on FRP, natural stone and their adhesive interface," *Composites Part B: Engineering,* vol. 80, pp. 162-176, 2015.

[35] H. Maljaee, B. Ghiassi, P. B. Lourenço and D. V. Oliveira, "Moisture-induced degradation of interfacial bond in FRP-strengthened masonry," *Composites Part B: Engineering,* vol. 87, pp. 47-58, 2016.

[36] B. Ghiassi, D. V. Oliveira and P. B. Lourenço, "Hygrothermal durability of bond in FRP-strengthened masonry," *Materials and structures,* vol. 47, no. 12, pp. 2039-2050, 2014.

[37] B. Ghiassi, G. Marcari, D. V. Oliveira and P. B. Lourenço, "Water degrading effects on the bond behavior in FRP-strengthened masonry," *Composites Part B: Engineering,* vol. 54, pp. 11-19, 2013.

[38] B. Ghiassi, P. B. Lourenço and D. V. Oliveira, "Accelerated hygrothermal aging of bond in FRP–masonry systems," *Journal of Composites for Construction,* vol. 19, no. 3, p. 04014051, 2015.

[39] B. Ghiassi, S. M. Silva, D. V. Oliveira, P. B. Lourenço and L. Bragança, "FRP-to-masonry bond durability assessment with infrared thermography method," *Journal of Nondestructive Evaluation,* vol. 33, no. 3, pp. 427-437, 2014.

[40] F. Ceroni, A. Bonati, V. Galimberti and A. Occhiuzzi, "Effects of environmental conditionings on the bond behavior of FRP and FRCM systems applied over concrete elements," *Journal of Engineering Mechanics,* vol. 144, no. 1, p. 04017144, 2018.

[41] N. Cavalagli, A. Kita, V. L. Castaldo, A. L. Pisello and F. Ubertini, "Hierarchical environmental risk mapping of material degradation in historic masonry buildings: An integrated approach considering climate change and structural damage," *Construction and Building Materials,* vol. 215, p. 998–1014, 2019.

[42] A. Bonazza, P. Messina, C. Sabbioni, C. M. Grossi and P. Brimblecombe, "Mapping the impact of climate change on surface recession of carbonate buildings in Europe," *Science of the total environment,* vol. 407, no. 6, pp. 2039-2050, 2009.

[43] B. Ghiassi, P. B. Lourenço and D. V. Oliveira, "Effect of environmental aging on the numerical response of FRP-strengthened masonry walls," *Journal of Structural Engineering,* vol. 142, no. 1, p. 04015087, 2015.

[44] A. M. D'Altri, F. Messali, J. Rots, G. Castellazzi and S. de Miranda, "A damaging block-based model for the analysis of the cyclic behaviour of full-scale masonry structures," *Engineering Fracture Mechanics,* vol. 209, pp. 423-448, 2019.

[45] G. Milani, T. Rotunno, E. Sacco and A. Tralli, "Failure load of FRP strengthened masonry walls: Experimental results and numerical models," *Structural Durability & Health Monitoring,* vol. 2, pp. 29-50, 2006.

[46] M. Accardi, C. Cucchiara, A. Failla and L. La Mendola, "CFRP flexural strenghtening of masonry walls: experimental and analytical approach," in *FRPRCS-8, 8th International Symposium on Fiber Reinforcement for Concrete Structures*, Patras, Greece, 2007.

[47] J. Lee and G. L. Fenves, "Plastic-Damage Model for Cyclic Loading of Concrete Structures," *Journal of Engineering Mechanics,* vol. 124, no. 8, p. 892–900, 1998 doi:10.1061/(asce)0733-9399(1998)124:8(892).

[48] G. Milani, M. Valente and C. Alessandri, "The Narthex of the Church of the Nativity in Bethlehem: A Non-Linear Finite Element Approach to Predict the Structural Damage," *Computers & Structures,* 2017 doi:10.1016/j.compstruc.2017.03.010.

[49] *Abaqus®. Theory manual, Version 6.17, 2017.*

[50] G. Milani and P. B. Lourenço, "Simple homogenized model for the nonlinear analysis of FRP-strengthened masonry structures. I: Theory," *Journal of Engineering Mechanics,* vol. 139, no. 1, pp. 59-76, 2013.

[51] M. Corradi, G. Castori, R. Sisti, A. Borri and G. L. Pesce, "Repair of Block Masonry Panels with CFRP Sheets," *Materials,* vol. 12, no. 15, p. 2363, 2019.

[52] A. Borri, M. Corradi, R. Sisti, C. Buratti, E. Belloni and E. Moretti, "Masonry wall panels retrofitted with thermal-insulating GFRP-reinforced jacketing," *Materials and Structures,* vol. 49, no. 10, pp. 3957-3968, 2016.

[53] M. A. ElGawady, P. Lestuzzi and M. Badoux, "Aseismic retrofitting of unreinforced masonry walls using FRP," *Composites Part B: Engineering,* vol. 37, no. 2-3, pp. 148-162, 2005.

[54] C. Papanicolaou, T. Triantafillou and M. Lekka, "Externally bonded grids as strengthening and seismic retrofitting materials of masonry panels," *Construction and Building Materials,* vol. 25, no. 2, pp. 504-514, 2011.

[55] L. La Mendola, A. Failla, C. Cucchiara and M. Accardi, "Debonding phenomena in CFRP strengthened calcarenite masonry walls and vaults," *Advances in Structural Engineering,* vol. 12, no. 5, pp. 745-760, 2009.

[56] L. La Mendola, M. Accardi, C. Cucchiara and V. Licata, "Nonlinear FE analysis of out-of-plane behaviour of masonry walls with and without CFRP reinforcement," *Construction and Building Materials,* vol. 54, pp. 190-196, 2014.

[57] A. Monaco, G. Minafò, C. Cucchiara, J. D'Anna and L. La Mendola, "Finite element analysis of the out-of-plane behavior of FRP strengthened masonry panels," *Composites Part B: Engineering,* vol. 115, pp. 188-202, 2017.

[58] M. Accardi, "Strengthening of masonry structural elements subjected to out-of-plane loads using CFRP Reinforcement," Doctoral dissertation, Phd Thesis, Palermo, Italy, 2004.

[59] E. Grande, G. Milani and E. Sacco, "Modelling and analysis of FRP-strengthened masonry panels," *Engineering Structures,* vol. 30, no. 7, pp. 1842-1860, 2008.

[60] E. Grande, M. Imbimbo and E. Sacco, "Finite element analysis of masonry panels strengthened with FRPs," *Composites Part B: Engineering,* vol. 45, no. 1, pp. 1296-1309, 2013.

[61] G. Milani and P. Lourenço, "Simple Homogenized Model for the Nonlinear Analysis of FRP-Strengthened Masonry Structures. II: Structural Applications," *Journal of Engineering Mechanics,* vol. 139, no. 1, pp. 77-93, 2013.

[62] G. Castellazzi, S. de Miranda, G. Formica, L. Molari and F. Ubertini, "Coupled hygro-mechanical multiscale analysis of masonry walls," *Engineering Structures,* vol. 84, pp. 266-278, 2015.

[63] M. Uranjek and V. Bokan-Bosiljkov, "Influence of freeze–thaw cycles on mechanical properties of historical brick masonry," *Construction and building Materials,* vol. 84, pp. 416-428, 2015.

[64] L. Niu, S. Zheng, H. Zheng, Y. Zhou and P. Pei, "Seismic behavior of confined masonry walls subjected to freeze-thaw cycles," *Construction and Building Materials,* vol. 186, pp. 131-144, 2018.

[65] R. Esposito, K. Terwel, G. Ravenshorst, H. Shipper, F. Messali and J. Rots, "Cyclic pushover test on an unreinforced masonry structure reseambling a typical Dutch terraced house," in *16th World Conference on Earthquake*, Santiago, Chile, 2017.

[66] R. Esposito, F. Messali, G. J. Ravenshorst, H. R. Schipper and J. G. Rots, "Seismic assessment of a lab-tested two-storey unreinforced masonry Dutch terraced house," *Bulletin of Earthquake Engineering,* pp. 1-23, 2019.

[67] F. Messali, R. Esposito, S. Jafari, G. Ravenshorst, P. Korswagen and J. Rots, "A multiscale experimental characterization of Dutch unreinforced masonry buildings," in *16th European Conference on Earthquake Engineering*, Thessaloniki, Greece, 2018.

[68] G. Castellazzi, C. Colla, S. de Miranda, G. Formica, E. Gabrielli, L. Molari and F. Ubertini, "A coupled multiphase model for hygrothermal analysis of masonry structures and prediction of stress induced by salt crystallization," *Construction and Building Materials,* vol. 41, p. 717–731, 2013.